Mixing state of oxalic acid containing particles in the rural area of Pearl River Delta, China: implications for the formation mechanism of oxalic acid

Chunlei Cheng[1,2], Mei Li[1,2*], Chak K. Chan[3], Haijie Tong[4], Changhong Chen[5], Duohong Chen[6], Dui Wu[1,2], Lei Li[1,2], Cheng Wu[1,2], Peng Cheng[1,2], Wei Gao[1,2], Zhengxu Huang[1,2], Xue Li[1,2], Zhijuan Zhang[1,2], Zhong Fu[7], Yanru Bi[7], Zhen Zhou[1,2*]

[1]Institute of Mass Spectrometer and Atmospheric Environment, Jinan University, Guangzhou 510632, China
[2]Guangdong Provincial Engineering Research Center for on-line source apportionment system of air pollution, Guangzhou 510632, China
[3]School of Energy and Environment, City University of Hong Kong, Hong Kong, China
[4]Max Planck Institute for Chemistry, Multiphase Chemistry Department, Hahn-Meitner-Weg 1, 55128 Mainz, Germany
[5]State of Environmental Protection Key Laboratory of the formation and prevention of urban air pollution complex, Shanghai Academy of Environmental Sciences, Shanghai 200233, China
[6] State Environmental Protection Key Laboratory of Regional Air Quality Monitoring, Guangdong Environmental Monitoring Center, Guangzhou, 510308, China
[7]Guangzhou Hexin Analytical Instrument Limited Company, Guangzhou 510530, China

Correspondence to: Mei Li (limei2007@163.com) and Zhen Zhou (zhouzhen@gig.ac.cn)
Tel: 86-20-85225991, Fax: 86-20-85225991

Abstract:

The formation of oxalic acid and its mixing state in atmospheric particulate matter (PM) were studied using a single particle aerosol mass spectrometer (SPAMS) in the summer and winter of 2014 in Heshan, a supersite in the rural area of the Pearl River Delta (PRD) region in China. Oxalic acid-containing particles accounted for 2.5% and 2.7% in total detected ambient particles in summer and winter, respectively. Oxalic acid was measured in particles classified as elemental carbon (EC), organic carbon (OC), elemental and organic carbon (ECOC), biomass burning (BB), heavy metal (HM), secondary (Sec), sodium-potassium (NaK) and dust. Oxalic acid was found predominantly mixing with sulfate and nitrate during the whole sampling period, likely due to aqueous phase reactions. In summer, oxalic acid-containing particle number and ozone concentration followed a very similar trend, which may reflect the significant contribution of photochemical reactions to oxalic acid formation. The HM type particles were the most abundant oxalic acid particles in summer and the diurnal variations of peak area of iron and oxalic acid show opposite trends, which suggest a possible loss of oxalic acid through the photolysis of iron oxalato complexes during the strong photochemical activity period. In wintertime, carbonaceous type particles contained a substantial amount of oxalic acid as well as abundant carbon clusters and biomass burning markers. The general existence of nitric acid in oxalic acid-containing particles indicates an acidic environment during the formation process of oxalic acid. The peak areas of nitrate, sulfate and oxalic had similar temporal change in the carbonaceous type oxalic acid particles, and the organosulfate-containing oxalic acid particles well correlated with total oxalic acid particles during the episode, which suggests the formation of oxalic acid is closely associated with the oxidation of organic precursors in aqueous phase.

Keywords: Oxalic acid; Single particles; Mixing state; Photochemical process; Aqueous phase reactions.

1. Introduction

Organic aerosol, typically a large fraction of fine particles, contains more than thousands of organic compounds and contributes to visibility reduction, photochemical smog, climate change and adverse health effects (Novakov and Penner, 1993;Goldstein and Galbally, 2007;Jimenez et al., 2009;Poschl and Shiraiwa, 2015). A significant component of organic aerosol is secondary organic aerosol (SOA) formed from the gas phase oxidation of volatile organic compounds (VOCs) followed by partitioning of products into particles or from heterogeneous reactions of VOCs with particles (Hallquist et al., 2009;Zhang et al., 2015). Dicarboxylic acids (DCAs) are abundant and ubiquitous constituents in SOA and can be effective tracers for the oxidative processes leading to the formation of SOA (Kawamura and Ikushima, 1993;Ervens et al., 2011;Wang et al., 2012;Cheng et al., 2013). DCAs normally have high water solubility and low vapor pressure, so they play important roles in controlling the hygroscopic properties of organic aerosols (Prenni et al., 2003;Ma et al., 2013) and activating cloud condensation nuclei (Booth et al., 2009). The primary emissions of DCAs from anthropogenic sources in urban areas are minor (Huang and Yu, 2007;Stone et al., 2010), and they are mainly derived from secondary oxidation of VOCs and subsequent intermediates (Ho et al., 2010;Myriokefalitakis et al., 2011). High concentrations of DCAs have been observed in biomass burning plume (Kundu et al., 2010;Kawamura et al., 2013) with more than 70% of DCAs produced from photochemical oxidation of water-soluble organic compounds, and only a small contribution from direct biomass burning emission (van Pinxteren et al., 2014).

The production of DCAs through photochemical reactions has been reported in many field studies via the analysis of the diurnal and seasonal variations of DCA(Kawamura and Ikushima, 1993;Kawamura and Yasui, 2005;Aggarwal and Kawamura, 2008;Pavuluri et al., 2010;Ho et al., 2011;Wang et al., 2017), but the mechanism of DCAs formation is still not well understood. Oxalic acid is usually the most abundant DCA observed in the field (Kawamura et al., 2004;Ho et al., 2007;Kawamura et al., 2010). A number of ground based and airborne field studies

have found a tight correlation between oxalic acid and sulfate in ambient particles and cloud droplets, relating aqueous phase chemistry to the formation of oxalic acid in aerosols and cloud droplets (Yao et al., 2002;Yao et al., 2003;Yu et al., 2005;Sorooshian et al., 2006;Sorooshian et al., 2007a;Sorooshian et al., 2007b;Miyazaki et al., 2009;Wonaschuetz et al., 2012;Wang et al., 2016). In recent years, several model and laboratory studies suggested that the aqueous phase oxidation of highly water-soluble organics like glyoxal, methylglyoxal and glyoxylic acid can efficiently produce oxalic acid in aerosol particles and cloud droplets (Lim et al., 2010;Myriokefalitakis et al., 2011;Ervens et al., 2014;Yu et al., 2014;McNeill, 2015). Recent stable carbon isotope studies and field observations have also suggested that oxalic acid forms through aqueous phase reactions (Wang et al., 2012;Cheng et al., 2015). However, the formation process of oxalic acid in ambient aerosols is still associated with great uncertainty due to the oxidation rates of precursors and oxidant levels in photochemistry and aqueous phase chemistry, which needs to be further studied.

Online measurements of the size distribution of oxalic acid-containing particles and the mixing state of oxalic acid with other compounds in aerosols are useful to examine the formation and evolution of oxalic acid and SOA particles. Sullivan and Prather investigated the diurnal cycle and mixing state of DCA-containing particles in Asian aerosol outflow using aerosol time-of-flight mass spectrometry (ATOFMS), and proposed the formation of DCA on Asian dust (Sullivan and Prather, 2007a). In addition, Yang et al. (2009) measured oxalic acid particles in Shanghai and proposed that in-cloud processes and heterogeneous reactions on hydrated aerosols contributed to the formation of oxalic acid (Yang et al., 2009). While the formation mechanism of oxalic acid especially in urban areas is still not clear, online measurements of the mixing state of oxalic acid provide a powerful tool to better understand the formation of oxalic acid in aerosol particles and cloud droplets.

The Pearl River Delta (PRD) region has distinct meteorological seasonality under the influence of the Asian monsoon system, which brings air from the ocean in spring and summer, and carries polluted air from northern China in autumn and winter.

Strong photochemical activity occurs in summer under the condition of high temperature and relative humidity, and in winter high loadings of particles from northern cities are favorable for the occurrence of haze episode (Bi et al., 2011;Zhang et al., 2013;Zhang et al., 2014). Here we present the seasonal field measurements of the mixing state of oxalic acid-containing particles using a single particle aerosol mass spectrometer (SPAMS) in a rural supersite of the PRD region. The seasonal characteristic of oxalic acid particles and mixing state with secondary species were investigated to explore the formation mechanisms of oxalic acid and aging process of SOA.

2. Methods

2.1 Aerosol sampling

Particles were sampled using a single particle aerosol mass spectrometer (SPAMS) at the Guangdong Atmospheric Supersite (22.73N, 112.93E), a rural site at Heshan city (Figure S1). The supersite is surrounded by farm land and villages, with no local industrial or traffic emissions. Ambient aerosols were sampled to the SPAMS through a 2.5m long copper tube with 0.5m of the sampling inlet located above the top of the building. The measurement period was from July 18 to August 1 in 2014, and from January 27 to February 8 in 2015. Real-time $PM_{2.5}$ mass concentration was simultaneously measured by a TEOM monitor (series 1405, Thermo scientific), and hourly concentrations of O_3 were measured by an O_3 analyzer (model 49i, Thermo scientific). The local meteorological data including temperature, relative humidity and visibility were measured on the rooftop of the building. The average temperature during the field study was 29.5℃ in summer and 14.1℃ in winter and the average relative humidity was 71.7% and 63% in summer and winter, respectively.

2.2 SPAMS

Real-time measurements of single atmospheric particles has been demonstrated by Prather and co-workers in the 1990s using aerosol time-of-flight mass spectrometry (ATOFMS) (Prather et al., 1994;Noble and Prather, 1996). Based on the same principle, the single particle aerosol mass spectrometer (SPAMS) developed by

Guangzhou Hexin Analytical Company was applied to field measurements of single particles in the current work. The details of the SPAMS system have been introduced previously (Li et al., 2011). Briefly, aerosol particles are sampled into the vacuum pumped aerodynamic lens of the SPAMS through an electro-spark machined 80μm critical orifice at a flow rate of 75 ml min^{-1}. The individual particles with a terminal velocity are introduced to the sizing region. The velocity of each single particle is detected by two continuous laser beams (diode Nd:YAG, 532 nm) with a space of 6 cm. The velocity is then used to calculate the single particle aerodynamic diameter and provide the precise timing of the firing of a 266 nm laser used to induce desorption and ionization (Nd:YAG laser, 266nm). The energy of the desorption/ionization 266 nm laser was 0.6 mJ and the power density was kept at about 1.6×10^{8} W/cm^{2} during both sampling periods. The 266 nm laser generates positive and negative ions that are detected by a Z-shaped bipolar time of flight mass spectrometer. The size range of the detected single particles is 0.2 to 2 μm. Polystyrene latex spheres (Nanosphere size standards, Duke Scientific Corp., Palo Alto) of 0.22-2.0 μm diameter were used for size calibration.

2.3 Data analysis

The size and chemical composition of single particles detected by SPAMS were analyzed using the COCO toolkit based on the Matlab software. Particles were clustered into several groups using the neural network algorithm (ART-2a) to group particles into clusters with similar mass spectrum features. The ART-2a parameters used in this work were set to a vigilance factor of 0.8, a learning rate of 0.05, and a maximum of 20 iterations. We collected 516,679 and 767,986 particles with both positive and negative mass spectra in summer and winter respectively. A standard solution of oxalic acid was prepared with pure oxalic acid ($H_2C_2O_4$, purity: 99.99%, Aladdin Industrial Corporation) and atomized to aerosols. After drying through two silica gel diffusion driers, pure oxalic acid particles were directly introduced into the SPAMS. The positive and negative mass spectra of oxalic acid are shown in Figure S2. Based on the mass spectra of pure oxalic acid and previous ambient measurements by ATOFMS (Silva and Prather, 2000;Sullivan and Prather, 2007a;Yang et al., 2009),

$HC_2O_4^-$ (m/z -89) is selected as the ion peak for oxalic acid containing particles. In this work, oxalic acid particles are identified if the peak area of m/z -89 was larger than 0.5% of the total signal in the mass spectrum. With this threshold, 13109 and 20504 of oxalic acid-containing particles were obtained in summer and winter separately, accounting for 2.5% and 2.7% of the total detected particles. The percentage of oxalic acid-containing particles in total particles in this work was comparable to the reported value in the urban area of Shanghai (3.4%) (Yang et al., 2009). However, these percentages are in general much lower than those reported in cleaner environments such as the western Pacific Ocean where oxalic acid was found in up to 1-40% of total particles due to little anthropogenic influences (Sullivan and Prather, 2007a).

The oxalic acid containing particles are classified into eight types in the following order: elemental carbon (EC), organic carbon (OC), elemental and organic carbon (ECOC), biomass burning (BB), heavy metal (HM), secondary (Sec), sodium-potassium (NaK) and dust. Different type particles are identified according to characteristic ion markers and dominant chemical species (Table S1): (1) particles containing abundant carbon clusters like $\pm12[C]^{+/-}$, $\pm24[C_2]^{+/-}$, $\pm36[C_3]^{+/-}$ with relative peak area more than 0.5% are classified as EC type, (2) any remaining particles containing abundant signals of $27[C_2H_3]^+$, $43[C_2H_3O]^+$ and hydrocarbon clusters with relative peak area more than 0.5% are classified as OC type, (3) any remaining particles containing signals of $\pm12[C]^{+/-}$, $\pm24[C_2]^{+/-}$, $37[C_3H]^+$ and $43[C_2H_3O]^+$ with relative peak area more than 0.5% are classified as ECOC type, (4) any remaining particles containing abundant signals of $39[K]^+$ (peak area>1500) with relative peak area of $-59[C_2H_3O_2]^-$ and $-73[C_3H_5O_2]^-$ simultaneously more than 0.5% are classified as BB type, (5) any remaining particles containing signals of $55[Mn]^+$, $56[Fe]^+$, $63/65[Cu]^+$, $64[Zn]^+$ and $208[Pb]^+$ with relative peak area more than 0.5% are classified as HM type, (6) any remaining particles containing abundant signals of $18[NH_4]^+$ (peak area>50), $-62[NO_3]^-$ (peak area>100) and $-97[HSO_4]^-$ (peak area>100) are classified as Sec type, (7) any remaining particles containing abundant signals of $23[Na]^+$ (peak area>1500) and related species are classified as NaK type, (8) any

remaining particles containing signals of 40[Ca]$^+$, 56[CaO]$^+$ and related species are classified as dust type. The rules for oxalic acid particles classification in the current work have been reported in previous studies (Sullivan and Prather, 2007b;Yang et al., 2009;Zhang et al., 2013;Li et al., 2014).

2.4 Inorganic ions and in-situ pH (pH_{is})

Water-soluble inorganic ions and trace gases were determined by an online analyzer for monitoring aerosols and gases (MARGA, model ADI 2080, Applikon Analytical B. V. Corp., the Netherlands) with a $PM_{2.5}$ sampling inlet at one hour resolution from July 18 to August 1 in 2014. The principle and instrumental design has been described in detail elsewhere (ten Brink et al., 2007;Du et al., 2011;Behera et al., 2013;Khezri et al., 2013). Standard solutions containing all detected ions were injected into MARGA before and after the field measurement. The liquid water content and the concentration of H^+ in particles are calculated using the ISORROPIA II model (Nenes et al., 1998, 1999;Fountoukis and Nenes, 2007). We choose stable mode and reverse type in the ISORROPIA model to calculate the concentration of H^+ and the liquid water content in this work. The in-situ pH (pH_{is}) of particles is calculated through the following equation:

$$pH_{is} = -\log\alpha_{H^+} = -\log(\gamma_{H^+} \times n_{H^+} \times 1000/V_a) \quad (1)$$

where n_{H^+} is the concentration of H^+ (mol m^{-3}) and V_a is the volume concentration of the H_2O (cm^3 m^{-3}) , while γ_{H^+} is the activity coefficient of H^+(Xue et al., 2011;Cheng et al., 2015). The temporal variation of pH_{is} of ambient $PM_{2.5}$ particles is presented in Figure S3, and demonstrated that 97% of particles were acidic in summer.

3. Results and Discussion

3.1 Seasonal variation of oxalic acid containing particles

The clustered 48 hr back trajectories of air masses arriving in Heshan during the sampling period are shown in Figure S4. In summer, air masses at 500m levels above the ground were mainly from the ocean and rural areas with less influence of human activity, while in winter air masses were directly from urban areas of Guangzhou and

Foshan, indicating a strong influence from anthropogenic emissions. The temporal variations of the total detected particles and oxalic acid containing particles in summer and winter are shown in Figure 1. The total particles had similar trends with the mass concentration of ambient $PM_{2.5}$, suggesting that the counts of total particles detected by SPAMS can be representative of $PM_{2.5}$ mass concentration during the whole sampling periods. The oxalic acid (C_2-containing) particles, in general, exhibited distinct diurnal peaks from July 28 to August 1, while they showed different temporal trends in winter. The relative abundance of oxalic acid particles in all of the sampled particles (C_2/total ratio) had the same variation with the abundance of oxalic acid particles in summer, especially in the period of July 28 – August 1 (Figure 1). In winter, however, particle counts and relative abundance of oxalic acid had different temporal changes except Jan 30 and February 5-8, when the count and relative abundance of oxalic acid particles simultaneously had a sudden increase.

The oxalic acid-containing particles were clustered into eight groups, and they altogether accounted for 89.6% and 95.1% of total oxalic acid particles in summer and winter, respectively. Table 1 shows that in summer heavy metal (HM) type particles contributed 31.3% to total oxalic acid particles, followed by the Sec (19.2%) and BB type (13%). However, in winter BB type particles were the most abundant and accounted for 24.2% of the oxalic acid-containing particles, followed by EC and HM type. Besides, carbonaceous type particles including EC, OC, ECOC and BB accounted for 28.1% of oxalic acid particles in summer and 59.8% in winter, indicating the seasonal different characteristics of oxalic acid particles. The temporal variations of eight groups of oxalic acid particles in summer and winter are illustrated in Figure 1. In summer HM type particles (orange color) and total oxalic acid particles exhibited similar diurnal patterns, suggesting a possible connection between the production of oxalic acid and the transition metals (e.g. Fe, Cu) (Zhou et al., 2015). Although Sec, BB and EC type particles showed similar diurnal patterns with total oxalic acid particles, the concentrations of these type particles were generally lower than HM type particles. In winter diurnal variation of oxalic acid particles was not obvious but a sharp increase, accompanied by the increase of BB, EC and Sec type

particles, was observed on February 8.

The averaged positive and negative ion mass spectra of oxalic acid containing particles are shown in Figure 2. The positive ion spectrum of oxalic acid particles in summer was characterized by high fractions of metal ion peaks including 23$[Na]^+$, 27$[Al]^+$, 39$[K]^+$, 55$[Mn]^+$, 56$[Fe]^+$, 63/65$[Cu]^+$, 64$[Zn]^+$ and 208$[Pb]^+$, and carbonaceous marker ions at m/z 27$[C_2H_3]^+$, 36$[C_3]^+$, 43$[C_2H_3O/C_3H_7]^+$, 48$[C_4]^+$ (Figure 2 a). The negative ion spectrum of oxalic acid particles in summer was characterized by the strong intensity of secondary ions including m/z -46$[NO_2]^-$, -62$[NO_3]^-$, -79$[PO_3]^-$, -80$[SO_3]^-$, -96$[SO_4]^-$ and -97$[HSO_4]^-$, as well as carbon clusters of -24$[C_2]^-$, -36$[C_3]^-$, -48$[C_4]^-$ and BB markers of -59$[C_2H_3O_2]^-$ and -73$[C_3H_5O_2]^-$ (Figure 2 b) (Zauscher et al., 2013). More carbonaceous clusters, i.e., 27$[C_2H_3]^+$, 29$[C_2H_5]^+$, 36$[C_3]^+$, 37$[C_3H]^+$, 43$[C_2H_3O]^+$, 48$[C_4]^+$, 51$[C_4H_3]^+$, 55$[C_4H_7]^+$, 60$[C_5]^+$, 63$[C_5H_3]^+$, 65$[C_5H_5]^+$, 74$[C_2H_2O_3]^+$, 77$[C_6H_5]^+$, were observed in the positive ion spectrum of oxalic acid particles in winter (Figure 2 c) than in summer. The negative ion spectrum of oxalic acid particles in winter (Figure 2 d) contained a large amount of secondary ions, similar to those found in summer, and a more intense signal of nitric acid (-125$[HNO_3NO_3]^-$) , suggesting an acidic nature of oxalic acid particles in winter.

The mixing state of oxalic acid particles with sulfate, nitrate and ammonium (SNA) was investigated through the percentage of SNA-containing oxalic acid particles in total oxalic acid particles (Figure 3). Oxalic acid was found to be internally mixed with sulfate and nitrate during both sampling periods with percentage of 93% and 94% in summer respectively, and both 98% in winter (Figure 3 a). However, the NH_4^+-containing oxalic acid particle (C_2-NH_4^+) only accounted for 18% of total oxalic acid particles in summer but this fraction increased to 71% in winter, and linear correlation between C_2-NH_4^+ particles and total oxalic acid particles showed better linear regression (r^2=0.98) in winter than summer, indicating a general mixing state of NH_4^+ with oxalic acid in winter. Aqueous phase production of SO_4^{2-} has been studied well and the linear correlation between oxalic acid and SO_4^{2-} has been used to study the production of oxalic acid through aqueous phase reactions (Yu

et al., 2005;Miyazaki et al., 2009;Cheng et al., 2015). In our work, oxalic acid and C_2-SO_4^{2-} displayed good correlations in summer and winter (both r^2=0.99), which suggests a common production route of oxalic acid and sulfate, likely aqueous phase reactions.

Figure 4 shows the unscaled size-resolved number distributions of the eight types of oxalic acid particles. Oxalic acid mainly existed in 0.4 to 1.2 μm particles during the entire sampling period but exhibited different peak modes for each particle type in summer and winter. In summer, major types of oxalic acid particles showed distinct peak mode at different size diameter. EC and Sec type particles peaked at 0.5 μm, followed by BB type particles at 0.55 μm, then HM type particles at 0.6 μm, and OC type particles at 0.7 μm. The difference of peak mode suggests the possible different chemical evolution process for each type oxalic acid-containing particles. However, in winter, oxalic acid particles showed broader size distribution from 0.5 to 0.8 μm for all particle types. Oxalic acid particles of all types were generally larger in winter than summer, possibly due to condensation and coagulation of particles during aging of oxalic acid particles in winter.

3.2 Photochemical production of oxalic acid in summer

In summer oxalic acid particles showed peaks in the afternoon especially from July 28 to August 1, which was in agreement with the variation pattern of the O_3 concentration (Figure 5), indicating a strong association of oxalic acid formation with photochemical reactions. Malonic acid is another product of photochemical oxidation of organic compounds (Kawamura and Ikushima, 1993;Wang et al., 2012;Meng et al., 2013;Meng et al., 2014). In our campaign, malonic acid containing particles had diurnal trends similar to oxalic acid particles and O_3 concentration. As the dominant particle type, HM particles had identical variation pattern with total oxalic acid particles. They are characterized by highly abundant metal ion peaks like 55$[Mn]^+$, 56$[Fe]^+$, 63/65$[Cu]^+$, 64$[Zn]^+$ and 208$[Pb]^+$, as well as secondary ion peaks of -46$[NO_2]^-$, -62$[NO_3]^-$, -80$[SO_3]^-$, -96$[SO_4]^-$ and -97$[HSO_4]^-$ in the negative spectrum in summer (Figure 6). In order to investigate the photochemical formation of oxalic acid in summer, the diurnal variations of O_3, oxalic acid particles, HM type particles

and pH_{is} of ambient particles averaged from July 28 to August 1, 2014 are shown in Figure 7. The concentration of O_3 increased after 9:00 and peaked at 17:00, while oxalic acid particles and HM type particles both increased after 10:00 and showed two peaks at 15:00 and 19:00. The pH_{is} of ambient particles ranging from -1.42 to 4.01 indicated an acidic environment, and the temporal trends of RH, inorganic ions and H^+ (aq) in aerosols are shown in Figure S5. The oxidation of glyoxal and glyoxylic acid by •OH has been identified as an important pathway of oxalic acid production by field and laboratory studies (Ervens et al., 2004;Ervens and Volkamer, 2010;Wang et al., 2012;Wang et al., 2015). In summer strong photochemical activity and high O_3 concentrations in the afternoon lead to more production of dicarbonyls and aldehydes (e.g. glyoxal and methylglyoxal) from VOCs (Myriokefalitakis et al., 2011), which increases the precursors of oxalic acid. The aqueous phase oxidation of glyoxal can take place in both clouds and wet aerosols (Lim et al., 2010). However, the lower yield of oxalic acid from glyoxal in wet aerosols compared to in clouds has been reported in previous chamber experiments due to the formation of substantial amount of high molecular weight products such as oligomers in aerosol-related concentrations (Carlton et al., 2007;Tan et al., 2009). These findings may explain the lower peak of oxalic acid particles at 15:00 compared to that at 19:00. Besides, the precursors of oxalic acid such as glyoxylic acid have higher reaction rate with •OH in high pH solutions according to previous studies(Ervens et al., 2003;Herrmann, 2003;Cheng et al., 2015), and in this work the increase of pH_{is} was observed as the enhancement of oxalic acid particles in the afternoon (Figure 7), which suggests an efficient oxalic acid production from the oxidation of precursors.

The similar photochemical pattern of HM type particles with O_3 and total oxalic acid particles implies a possible participation of metal ions in the formation process of oxalic acid. The modeling studies from Ervens et al. (2014) suggest that oxalic acid production from glyoxal and glyoxylic acid in aqueous phase significantly depends on •OH availability (Ervens et al., 2014). The main sources of aqueous phase •OH in cloud droplets include direct uptake from the gas phase (Jacob, 1986), ozone photolysis by UV and visible light at the air-water interface (Anglada et al., 2014),

and also aqueous phase chemical reactions(Gligorovski et al., 2015). For the last kind of source, •OH radicals could be generated through Fenton or Fenton like reactions and photolysis of H_2O_2, NO_3^-, NO_2^-, and chromophoric dissolved organic matter (CDOM) (Badali et al., 2015;Ervens, 2015;Herrmann et al., 2015;Tong et al., 2016). Given that SPAMS cannot be used to quantify the concentrations of iron ions and H_2O_2, we will investigate the relative contribution of different source •OH radicals to the formation of oxalic acid and show results in our follow up studies.

The oxalic acid loss through the photolysis of iron oxalato complexes is a significant sink according to field measurements and model simulations (Sorooshian et al., 2013;Weller et al., 2014;Zhou et al., 2015). Considering the high abundance of iron in oxalic acid particles in the current work (Figure 6), the photolysis of iron oxalato complexes could have played an important role in the diurnal variation of oxalic acid particles. Because the mass concentration of Fe (III) and oxalic acid could not be obtained through SPAMS, the diurnal variations of peak area of iron (m/z=56) and oxalic acid (m/z=-89) were used to investigate the role of iron on the net production of oxalic in the HM type particles from July 28 to August 1, 2014 (Figure 8). Interestingly, the peak area of iron exhibited opposite trend with the peak area of oxalic acid from 4:00 to 11:00. As the peak area of Fe increased from 1565 to 29920 from 4:00 to 7:00, the peak area of oxalic decreased from 6052 to 3487 accordingly. From 8:00 to 11:00, the peak area of Fe had a very low value of 1168, but the peak area of oxalic had a very high value of 5538. In addition, the peak area of iron exhibited a high value of 138199 at 14:00, while the peak area of oxalic acid showed a lower peak of 7687 at 14:00 and a higher peak of 11879 at 19:00 with an extremely low abundance of iron. Above opposite variation patterns of iron and oxalic acid in iron rich HM type particles during the photochemical activity period from 5:00 to 19:00 strongly indicated that photolysis of iron oxalato complexes could be an efficient sink of oxalic acid.

The influence from traffic emission was investigated through the diurnal variations of total EC type particles and NO_2 (Figure S6). The EC type particles increased from 12:00 to 21:00, which had same variation as total oxalic acid, but NO_2

followed the rush hour pattern with two peaks from 5:00 to 8:00 and from 18:00 to 21:00. Traffic emission is not expected to have a large contribution to oxalic acid in this study. The wind speed was low during the whole day (Figure S6), especially between 9:00 and 18:00, which provided a stagnant environment for the increase in oxalic acid produced from photochemical process.

3.3 Formation process of oxalic acid in winter

Despite lower O_3 concentrations and photochemical activity in winter, oxalic acid was still prevalent in carbonaceous particles, especially BB type particles. While oxalic acid was found to be internally mixed with sulfate and nitrate both in summer and winter, the nitric acid was only observed in oxalic acid particles in winter, indicating a strongly acidic nature of oxalic acid particles in winter. Considering a possible connection of oxalic acid production with the acidic environment, the temporal concentrations of oxalic acid, sulfate and nitrate were investigated through their peak areas in the carbonaceous type oxalic acid particles including EC, OC, ECOC and BB type in Figure 9. The peaks of m/z -62$[NO_3]^-$ and - 97$[HSO_4]^-$ represent nitrate and sulfate, respectively. Nitrate, sulfate and oxalic acid showed very similar variation patterns in winter, suggesting a close connection of the formation of oxalic acid with the existence of nitrate and sulfate. Although nitric acid was found in the oxalic acid particles, the acidity of the oxalic acid particles was not estimated since the real-time concentration of inorganic ions was not available during the sampling period in winter. Instead the relative acidity ratio (R_{ra}), defined as the ratio of total peak areas of nitrate and sulfate to the peak area of ammonium (m/z 18$[NH_4]^+$), was used (Denkenberger et al., 2007;Pratt et al., 2009). The R_{ra} of carbonaceous type oxalic acid particles ranged from 7 to 114 with an average value of 25 (Figure 9), indicating an intensely acidic environment of carbonaceous type oxalic acid particles in winter. Several studies have reported the formation of oxalic acid through the oxidation of glyoxal and related precursors in acidic aqueous phase (Carlton et al., 2006;Carlton et al., 2007;Tan et al., 2009). Although the influence of different particle acidity on the oxidation process of glyoxal still needs evaluation, the moderate acidic environment is favorable for the production of oxalic acid from the

oxidation of glyoxal (Herrmann, 2003;Ervens and Volkamer, 2010;Eugene et al., 2016). In this work the acidic environment of the carbonaceous type oxalic acid particles and similar variation patterns among oxalic acid, sulfate and nitrate may suggest a relationship between the degradation of organic precursors and the acidic chemical process. However, the temporal change of R_{ra} did not follow a similar trend as the peak area of oxalic acid in most particles, possibly due to the multi-step formation of oxalic acid influenced by many factors such as precursors, liquid water content and ion strength (Carlton et al., 2007;Cheng et al., 2013;Cheng et al., 2015).

The sharp increase of oxalic acid particles on February 8, 2015 (Figure 1) was selected as a typical episode to investigate the formation processes of oxalic acid in winter. During the episode, the 48 hr back trajectory analysis showed air masses that originated from the urban areas of Guangzhou and Foshan city (Figure S4), indicating strong influence on organic precursors from anthropogenic emissions. Oxalic acid particle types were dominated by BB (23.2%), followed by EC (22.0%) and Sec (15.1%) type (Table 2). Carbonaceous particles including EC, ECOC, OC, BB accounted for 61.6% of the total oxalic acid particles. The mass spectra of oxalic acid particles were characterized by many hydrocarbon clusters of 27$[C_2H_3]^+$, 29$[C_2H_5]^+$, 37$[C_3H]^+$, 43$[C_2H_3O]^+$, 51$[C_4H_3]^+$, 55$[C_4H_7]^+$, 63$[C_5H_3]^+$, 65$[C_5H_5]^+$, 74$[C_2H_2O_3]^+$, 77$[C_6H_5]^+$, and carbon clusters of 36$[C_3]^+$, 48$[C_4]^+$, 60$[C_5]^+$ in positive mass spectrum, while the negative mass spectrum was characterized by elemental carbon clusters like -24$[C_2]^-$, -36$[C_3]^-$, -48$[C_4]^-$, biomass burning markers of -59$[C_2H_3O_2]^-$ and -73$[C_3H_5O_2]^-$ and secondary species including -42$[CNO]^-$, -46$[NO_2]^-$, -62$[NO_3]^-$, -79$[PO_3]^-$, -80$[SO_3]^-$, -96$[SO_4]^-$ and -97$[HSO_4]^-$ (Figure 10 a).

As the precursor of oxalic acid, glyoxal has the potential to react with sulfuric acid to produce organosulfates through acid-catalyzed nucleophilic addition according to laboratory and chamber studies(Surratt et al., 2007;Galloway et al., 2009). The negative ion of -155($[C_2H_3O_2SO_4]^-$) has been identified as the marker ion of organosulfates derived from glyoxal in chamber and field measurements using ATOFMS (Surratt et al., 2008;Hatch et al., 2011). The formation of organosulfates from glyoxal requires an acidic aqueous environment, which can be used as a marker

of acidic aqueous phase aging process of organic compounds. The temporal trend of organosulfate-containing oxalic acid particles in winter is shown in Figure S7, which exhibited a similar pattern as the total oxalic acid particles during the whole sampling period in winter. The percentage of organosulfate-containing oxalic acid particles in total oxalic acid particles ranged from 0 to 16.4% with the highest ratio observed in the episode (February 8). The linear regression between total oxalic acid particles and organosulfate-containing oxalic acid particles in the episode is exhibited in Figure 10b, and the robust correlation (r^2=0.81) between them suggests that oxalic acid and organosulfate may share similar formation process. Based on the above discussion, the degradation of carbonaceous species associated with acidic aqueous phase chemical reactions may have an important contribution to the formation of oxalic acid during the episode in winter. Similar particle types and mass spectra of oxalic acid-containing particles during the episode and the whole sampling period in winter were observed, which suggests the acidic aqueous phase chemical processing of organic precursors as a potential source for oxalic acid.

4. Summary and conclusions

Oxalic acid containing particles were measured by a single particle aerosol mass spectrometer (SPAMS) in the summer and winter of 2014 in Heshan, China. They accounted for 2.5% and 2.7% of the total detected ambient particles. In summer heavy metal-containing particles were the largest group of particles containing oxalic acid with a fraction of 31.3% followed by Sec type (19.2%), while in winter BB type was the dominant group with a percentage of 24.2%. More than 90% of oxalic acid particles were internally mixed with sulfate and nitrate during the whole sampling period. Only 18% of oxalic acid particles contained ammonium in summer, which increased to 71% in winter. In summer oxalic acid and O_3 concentration exhibited similar diurnal variations, indicating a substantial contribution of photochemical reactions to oxalic acid formation. The diurnal variations of peak area of iron and oxalic acid in HM type particles indicate a net production of oxalic acid at 15:00 lower than at 19:00, likely due to a significant loss of oxalic acid through the

photolysis of iron oxalato complexes during the strong photochemical activity period. In winter carbonaceous type particles including EC, OC, ECOC and BB groups accounted for 59.8% of oxalic acid particles and increased to 61.6% in the episode. Nitric acid and organosulfate were found to co-exist in oxalic acid-containing particles in the winter, which suggests a close association with acidic aqueous phase reactions. Acidic aqueous phase chemical processing of organic precursors is a potential contribution for the formation of oxalic acid in winter. The current study demonstrates that SPAMS is a unique tool for understanding the mixing states of different components of ambient aerosols, which are useful for exploring the formation and evolution process of SOA.

Acknowledgements

This work was financially supported by National Key Technology R&D Program (Grant No. 2014BAC21B01), Guangdong Province Public Interest Research and Capacity Building Special Fund (Grant No. 2014B020216005), the Strategic Priority Research Program (B) of the Chinese Academy of Sciences (Grant No. XDB05040502), Guangdong Industry-University Research Program (Grant No.2012B090500014), and NSFC of Guangdong Province (Grant No. 2015A030313339). Chak K. Chan would like to acknowledge funding support of the General Fund of National Natural Science Foundation of China (Grant No. 41675117). Haijie Tong acknowledge Max Planck Society for funding and Ulrich Pöschl for helpful discussions.

References

Aggarwal, S. G., and Kawamura, K.: Molecular distributions and stable carbon isotopic compositions of dicarboxylic acids and related compounds in aerosols from Sapporo, Japan: Implications for photochemical aging during long-range atmospheric transport, Journal of Geophysical Research-Atmospheres, 113, D14301, 10.1029/2007jd009365, 2008.

Anglada, J. M., Martins-Costa, M., Ruiz-López, M. F., and Francisco, J. S.: Spectroscopic signatures of ozone at the air–water interface and photochemistry implications, Proceedings of the National Academy of Sciences, 111, 11618-11623, 10.1073/pnas.1411727111, 2014.

Badali, K. M., Zhou, S., Aljawhary, D., Antinolo, M., Chen, W. J., Lok, A., Mungall, E., Wong, J. P. S., Zhao, R., and Abbatt, J. P. D.: Formation of hydroxyl radicals from photolysis of secondary organic aerosol material, Atmospheric Chemistry and Physics, 15, 7831-7840,

10.5194/acp-15-7831-2015, 2015.
Behera, S. N., Betha, R., Liu, P., and Balasubramanian, R.: A study of diurnal variations of PM 2.5 acidity and related chemical species using a new thermodynamic equilibrium model, Science of the Total Environment, 452, 286-295, 2013.
Bi, X., Zhang, G., Li, L., Wang, X., Li, M., Sheng, G., Fu, J., and Zhou, Z.: Mixing state of biomass burning particles by single particle aerosol mass spectrometer in the urban area of PRD, China, Atmospheric Environment, 45, 3447-3453, 2011.
Booth, A. M., Topping, D. O., McFiggans, G., and Percival, C. J.: Surface tension of mixed inorganic and dicarboxylic acid aqueous solutions at 298.15 K and their importance for cloud activation predictions, Phys Chem Chem Phys, 11, 8021-8028, 10.1039/b906849j, 2009.
Carlton, A. G., Turpin, B. J., Lim, H. J., Altieri, K. E., and Seitzinger, S.: Link between isoprene and secondary organic aerosol (SOA): Pyruvic acid oxidation yields low volatility organic acids in clouds, Geophysical Research Letters, 33, L06822, 10.1029/2005gl025374, 2006.
Carlton, A. G., Turpin, B. J., Altieri, K. E., Seitzinger, S., Reff, A., Lim, H. J., and Ervens, B.: Atmospheric oxalic acid and SOA production from glyoxal: Results of aqueous photooxidation experiments, Atmospheric Environment, 41, 7588-7602, 10.1016/j.atmosenv.2007.05.035, 2007.
Cheng, C., Wang, G., Meng, J., Wang, Q., Cao, J., Li, J., and Wang, J.: Size-resolved airborne particulate oxalic and related secondary organic aerosol species in the urban atmosphere of Chengdu, China, Atmospheric Research, 161, 134-142, 2015.
Cheng, C. L., Wang, G. H., Zhou, B. H., Meng, J. J., Li, J. J., Cao, J. J., and Xiao, S.: Comparison of dicarboxylic acids and related compounds in aerosol samples collected in Xi'an, China during haze and clean periods, Atmospheric Environment, 81, 443-449, 10.1016/j.atmosenv.2013.09.013, 2013.
Denkenberger, K. A., Moffet, R. C., Holecek, J. C., Rebotier, T. P., and Prather, K. A.: Real-time, single-particle measurements of oligomers in aged ambient aerosol particles, Environmental Science & Technology, 41, 5439-5446, 10.1021/es070329l, 2007.
Du, H., Kong, L., Cheng, T., Chen, J., Du, J., Li, L., Xia, X., Leng, C., and Huang, G.: Insights into summertime haze pollution events over Shanghai based on online water-soluble ionic composition of aerosols, Atmospheric Environment, 45, 5131-5137, 2011.
Ervens, B., Gligorovski, S., and Herrmann, H.: Temperature-dependent rate constants for hydroxyl radical reactions with organic compounds in aqueous solutions, Phys Chem Chem Phys, 5, 1811-1824, Doi 10.1039/B300072a, 2003.
Ervens, B., Feingold, G., Frost, G. J., and Kreidenweis, S. M.: A modeling study of aqueous production of dicarboxylic acids: 1. Chemical pathways and speciated organic mass production, Journal of Geophysical Research-Atmospheres, 109, D15205, 10.1029/2003jd004387, 2004.
Ervens, B., and Volkamer, R.: Glyoxal processing by aerosol multiphase chemistry: towards a kinetic modeling framework of secondary organic aerosol formation in aqueous particles, Atmospheric Chemistry and Physics, 10, 8219-8244, DOI 10.5194/acp-10-8219-2010, 2010.
Ervens, B., Turpin, B. J., and Weber, R. J.: Secondary organic aerosol formation in cloud droplets and aqueous particles (aqSOA): a review of laboratory, field and model studies, Atmospheric Chemistry and Physics, 11, 11069-11102, 10.5194/acp-11-11069-2011, 2011.
Ervens, B., Sorooshian, A., Lim, Y. B., and Turpin, B. J.: Key parameters controlling OH-initiated formation of secondary organic aerosol in the aqueous phase (aqSOA), Journal of Geophysical Research-Atmospheres, 119, 3997-4016, 10.1002/2013JD021021, 2014.

562 Ervens, B.: Modeling the Processing of Aerosol and Trace Gases in Clouds and Fogs, Chem Rev, 115,
563 4157-4198, 10.1021/cr5005887, 2015.
564 Eugene, A. J., Xia, S. S., and Guzman, M. I.: Aqueous Photochemistry of Glyoxylic Acid, Journal of
565 Physical Chemistry A, 120, 3817-3826, 10.1021/acs.jpca.6b00225, 2016.
566 Fountoukis, C., and Nenes, A.: ISORROPIA II: a computationally efficient thermodynamic equilibrium
567 model for K+–Ca 2+–Mg 2+–NH 4+–Na+–SO 4 2−–NO 3−–Cl−–H 2 O aerosols, Atmospheric
568 Chemistry and Physics, 7, 4639-4659, 2007.
569 Galloway, M. M., Chhabra, P. S., Chan, A. W. H., Surratt, J. D., Flagan, R. C., Seinfeld, J. H., and
570 Keutsch, F. N.: Glyoxal uptake on ammonium sulphate seed aerosol: reaction products and
571 reversibility of uptake under dark and irradiated conditions, Atmospheric Chemistry and Physics,
572 9, 3331-3345, 10.5194/acp-9-3331-2009, 2009.
573 Gligorovski, S., Strekowski, R., Barbati, S., and Vione, D.: Environmental Implications of Hydroxyl
574 Radicals (•OH), Chem Rev, 115, 13051-13092, 10.1021/cr500310b, 2015.
575 Goldstein, A. H., and Galbally, I. E.: Known and unexplored organic constituents in the earth's
576 atmosphere, Environmental Science & Technology, 41, 1514-1521, Doi 10.1021/Es072476p,
577 2007.
578 Hallquist, M., Wenger, J. C., Baltensperger, U., Rudich, Y., Simpson, D., Claeys, M., Dommen, J.,
579 Donahue, N. M., George, C., Goldstein, A. H., Hamilton, J. F., Herrmann, H., Hoffmann, T.,
580 Iinuma, Y., Jang, M., Jenkin, M. E., Jimenez, J. L., Kiendler-Scharr, A., Maenhaut, W., McFiggans,
581 G., Mentel, T. F., Monod, A., Prévôt, A. S. H., Seinfeld, J. H., Surratt, J. D., Szmigielski, R., and
582 Wildt, J.: The formation, properties and impact of secondary organic aerosol: current and
583 emerging issues, Atmospheric Chemistry and Physics, 9, 5155-5236, 10.5194/acp-9-5155-2009,
584 2009.
585 Hatch, L. E., Creamean, J. M., Ault, A. P., Surratt, J. D., Chan, M. N., Seinfeld, J. H., Edgerton, E. S.,
586 Su, Y., and Prather, K. A.: Measurements of isoprene-derived organosulfates in ambient aerosols
587 by aerosol time-of-flight mass spectrometry-Part 1: Single particle atmospheric observations in
588 Atlanta, Environmental science & technology, 45, 5105-5111, 2011.
589 Herrmann, H.: Kinetics of aqueous phase reactions relevant for atmospheric chemistry, Chem Rev, 103,
590 4691-4716, Doi 10.1021/Cr020658q, 2003.
591 Herrmann, H., Schaefer, T., Tilgner, A., Styler, S. A., Weller, C., Teich, M., and Otto, T.: Tropospheric
592 Aqueous-Phase Chemistry: Kinetics, Mechanisms, and Its Coupling to a Changing Gas Phase,
593 Chem Rev, 115, 4259-4334, 10.1021/cr500447k, 2015.
594 Ho, K. F., Cao, J. J., Lee, S. C., Kawamura, K., Zhang, R. J., Chow, J. C., and Watson, J. G.:
595 Dicarboxylic acids, ketocarboxylic acids, and dicarbonyls in the urban atmosphere of China,
596 Journal of Geophysical Research-Atmospheres, 112, D22S27, 10.1029/2006jd008011, 2007.
597 Ho, K. F., Lee, S. C., Ho, S. S. H., Kawamura, K., Tachibana, E., Cheng, Y., and Zhu, T.: Dicarboxylic
598 acids, ketocarboxylic acids, alpha-dicarbonyls, fatty acids, and benzoic acid in urban aerosols
599 collected during the 2006 Campaign of Air Quality Research in Beijing (CAREBeijing-2006),
600 Journal of Geophysical Research-Atmospheres, 115, D19312, 10.1029/2009jd013304, 2010.
601 Ho, K. F., Ho, S. S. H., Lee, S. C., Kawamura, K., Zou, S. C., Cao, J. J., and Xu, H. M.: Summer and
602 winter variations of dicarboxylic acids, fatty acids and benzoic acid in PM(2.5) in Pearl Delta
603 River Region, China, Atmospheric Chemistry and Physics, 11, 2197-2208,
604 10.5194/acp-11-2197-2011, 2011.
605 Huang, X.-F., and Yu, J. Z.: Is vehicle exhaust a significant primary source of oxalic acid in ambient

606 aerosols?, Geophysical Research Letters, 34, L02808, 10.1029/2006gl028457, 2007.
607 Jacob, D. J.: Chemistry of OH in remote clouds and its role in the production of formic acid and
608 peroxymonosulfate, Journal of Geophysical Research: Atmospheres, 91, 9807-9826,
609 10.1029/JD091iD09p09807, 1986.
610 Jimenez, J. L., Canagaratna, M. R., Donahue, N. M., Prevot, A. S. H., Zhang, Q., Kroll, J. H., DeCarlo,
611 P. F., Allan, J. D., Coe, H., Ng, N. L., Aiken, A. C., Docherty, K. S., Ulbrich, I. M., Grieshop, A. P.,
612 Robinson, A. L., Duplissy, J., Smith, J. D., Wilson, K. R., Lanz, V. A., Hueglin, C., Sun, Y. L.,
613 Tian, J., Laaksonen, A., Raatikainen, T., Rautiainen, J., Vaattovaara, P., Ehn, M., Kulmala, M.,
614 Tomlinson, J. M., Collins, D. R., Cubison, M. J., Dunlea, E. J., Huffman, J. A., Onasch, T. B.,
615 Alfarra, M. R., Williams, P. I., Bower, K., Kondo, Y., Schneider, J., Drewnick, F., Borrmann, S.,
616 Weimer, S., Demerjian, K., Salcedo, D., Cottrell, L., Griffin, R., Takami, A., Miyoshi, T.,
617 Hatakeyama, S., Shimono, A., Sun, J. Y., Zhang, Y. M., Dzepina, K., Kimmel, J. R., Sueper, D.,
618 Jayne, J. T., Herndon, S. C., Trimborn, A. M., Williams, L. R., Wood, E. C., Middlebrook, A. M.,
619 Kolb, C. E., Baltensperger, U., and Worsnop, D. R.: Evolution of Organic Aerosols in the
620 Atmosphere, Science, 326, 1525-1529, 10.1126/science.1180353, 2009.
621 Kawamura, K., and Ikushima, K.: seasonal-changes in the distribution of dicarboxylic-acids in the
622 urban atmosphere, Environmental Science & Technology, 27, 2227-2235, 10.1021/es00047a033,
623 1993.
624 Kawamura, K., Kobayashi, M., Tsubonuma, N., Mochida, M., Watanabe, T., and Lee, M.: Organic and
625 inorganic compositions of marine aerosols from East Asia: Seasonal variations of water-soluble
626 dicarboxylic acids, major ions, total carbon and nitrogen, and stable C and N isotopic composition,
627 Geochemical Investigations in Earth and Space Science: A Tribute to Issac R. Kaplan, 9, edited by:
628 Hill, R. J. L. J. A. Z. B. M. J. C. G., and Eganhouse, R. G. M. P. K., 243-265 pp., 2004.
629 Kawamura, K., and Yasui, O.: Diurnal changes in the distribution of dicarboxylic acids, ketocarboxylic
630 acids and dicarbonyls in the urban Tokyo atmosphere, Atmospheric Environment, 39, 1945-1960,
631 10.1016/j.atmosenv.2004.12.014, 2005.
632 Kawamura, K., Kasukabe, H., and Barrie, L. A.: Secondary formation of water-soluble organic acids
633 and alpha-dicarbonyls and their contributions to total carbon and water-soluble organic carbon:
634 Photochemical aging of organic aerosols in the Arctic spring, Journal of Geophysical
635 Research-Atmospheres, 115, D21306, 10.1029/2010jd014299, 2010.
636 Kawamura, K., Tachibana, E., Okuzawa, K., Aggarwal, S. G., Kanaya, Y., and Wang, Z. F.: High
637 abundances of water-soluble dicarboxylic acids, ketocarboxylic acids and alpha-dicarbonyls in the
638 mountaintop aerosols over the North China Plain during wheat burning season, Atmospheric
639 Chemistry and Physics, 13, 8285-8302, 10.5194/acp-13-8285-2013, 2013.
640 Khezri, B., Mo, H., Yan, Z., Chong, S.-L., Heng, A. K., and Webster, R. D.: Simultaneous online
641 monitoring of inorganic compounds in aerosols and gases in an industrialized area, Atmospheric
642 Environment, 80, 352-360, 2013.
643 Kundu, S., Kawamura, K., Andreae, T. W., Hoffer, A., and Andreae, M. O.: Molecular distributions of
644 dicarboxylic acids, ketocarboxylic acids and alpha-dicarbonyls in biomass burning aerosols:
645 implications for photochemical production and degradation in smoke layers, Atmospheric
646 Chemistry and Physics, 10, 2209-2225, 10.5194/acp-10-2209-2010, 2010.
647 Li, L., Huang, Z. X., Dong, J. G., Li, M., Gao, W., Nian, H. Q., Fu, Z., Zhang, G. H., Bi, X. H., Cheng,
648 P., and Zhou, Z.: Real time bipolar time-of-flight mass spectrometer for analyzing single aerosol
649 particles, Int J Mass Spectrom, 303, 118-124, 10.1016/j.ijms.2011.01.017, 2011.

Li, L., Li, M., Huang, Z., Gao, W., Nian, H., Fu, Z., Gao, J., Chai, F., and Zhou, Z.: Ambient particle characterization by single particle aerosol mass spectrometry in an urban area of Beijing, Atmospheric Environment, 94, 323-331, 2014.

Lim, Y. B., Tan, Y., Perri, M. J., Seitzinger, S. P., and Turpin, B. J.: Aqueous chemistry and its role in secondary organic aerosol (SOA) formation, Atmospheric Chemistry and Physics, 10, 10521-10539, 10.5194/acp-10-10521-2010, 2010.

Ma, Q. X., He, H., and Liu, C.: Hygroscopic properties of oxalic acid and atmospherically relevant oxalates, Atmospheric Environment, 69, 281-288, 10.1016/j.atmosenv.2012.12.011, 2013.

McNeill, V. F.: Aqueous organic chemistry in the atmosphere: Sources and chemical processing of organic aerosols, Environmental science & technology, 49, 1237-1244, 2015.

Meng, J. J., Wang, G. H., Li, J. J., Cheng, C. L., and Cao, J. J.: Atmospheric oxalic acid and related secondary organic aerosols in Qinghai Lake, a continental background site in Tibet Plateau, Atmospheric Environment, 79, 582-589, 10.1016/j.atmosenv.2013.07.024, 2013.

Meng, J. J., Wang, G. H., Li, J. J., Cheng, C. L., Ren, Y. Q., Huang, Y., Cheng, Y. T., Cao, J. J., and Zhang, T.: Seasonal characteristics of oxalic acid and related SOA in the free troposphere of Mt. Hua, central China: Implications for sources and formation mechanisms, Science Of The Total Environment, 493, 1088-1097, 10.1016/j.scitotenv.2014.04.086, 2014.

Miyazaki, Y., Aggarwal, S. G., Singh, K., Gupta, P. K., and Kawamura, K.: Dicarboxylic acids and water-soluble organic carbon in aerosols in New Delhi, India, in winter: Characteristics and formation processes, Journal of Geophysical Research-Atmospheres, 114, D19206, 10.1029/2009jd011790, 2009.

Myriokefalitakis, S., Tsigaridis, K., Mihalopoulos, N., Sciare, J., Nenes, A., Kawamura, K., Segers, A., and Kanakidou, M.: In-cloud oxalate formation in the global troposphere: a 3-D modeling study, Atmospheric Chemistry and Physics, 11, 5761-5782, 10.5194/acp-11-5761-2011, 2011.

Nenes, A., Pandis, S. N., and Pilinis, C.: ISORROPIA: A new thermodynamic equilibrium model for multiphase multicomponent inorganic aerosols, Aquatic geochemistry, 4, 123-152, 1998.

Nenes, A., Pandis, S. N., and Pilinis, C.: Continued development and testing of a new thermodynamic aerosol module for urban and regional air quality models, Atmospheric Environment, 33, 1553-1560, 1999.

Noble, C. A., and Prather, K. A.: Real-time measurement of correlated size and composition profiles of individual atmospheric aerosol particles, Environmental science & technology, 30, 2667-2680, 1996.

Novakov, T., and Penner, J. E.: Large Contribution of Organic Aerosols to Cloud-Condensation-Nuclei Concentrations, Nature, 365, 823-826, Doi 10.1038/365823a0, 1993.

Pavuluri, C. M., Kawamura, K., and Swaminathan, T.: Water-soluble organic carbon, dicarboxylic acids, ketoacids, and alpha-dicarbonyls in the tropical Indian aerosols, Journal of Geophysical Research-Atmospheres, 115, D11302, 10.1029/2009JD012661, 2010.

Poschl, U., and Shiraiwa, M.: Multiphase Chemistry at the Atmosphere-Biosphere Interface Influencing Climate and Public Health in the Anthropocene, Chem Rev, 115, 4440-4475, 10.1021/cr500487s, 2015.

Prather, K. A., Nordmeyer, T., and Salt, K.: Real-time characterization of individual aerosol particles using time-of-flight mass spectrometry, Anal. Chem., 66, 1403-1407, 1994.

Pratt, K. A., Hatch, L. E., and Prather, K. A.: Seasonal Volatility Dependence of Ambient Particle Phase Amines, Environmental Science & Technology, 43, 5276-5281, 10.1021/es803189n, 2009.

694 Prenni, A. J., De Mott, P. J., and Kreidenweis, S. M.: Water uptake of internally mixed particles
695 containing ammonium sulfate and dicarboxylic acids, Atmospheric Environment, 37, 4243-4251,
696 10.1016/s1352-2310(03)00559-4, 2003.
697 Silva, P. J., and Prather, K. A.: Interpretation of mass spectra from organic compounds in aerosol
698 time-of-flight mass spectrometry, Anal. Chem., 72, 3553-3562, 2000.
699 Sorooshian, A., Varutbangkul, V., Brechtel, F. J., Ervens, B., Feingold, G., Bahreini, R., Murphy, S. M.,
700 Holloway, J. S., Atlas, E. L., Buzorius, G., Jonsson, H., Flagan, R. C., and Seinfeld, J. H.: Oxalic
701 acid in clear and cloudy atmospheres: Analysis of data from International Consortium for
702 Atmospheric Research on Transport and Transformation 2004, Journal of Geophysical
703 Research-Atmospheres, 111, 10.1029/2005jd006880, 2006.
704 Sorooshian, A., Lu, M.-L., Brechtel, F. J., Jonsson, H., Feingold, G., Flagan, R. C., and Seinfeld, J. H.:
705 On the source of organic acid aerosol layers above clouds, Environmental Science & Technology,
706 41, 4647-4654, 10.1021/es0630442, 2007a.
707 Sorooshian, A., Ng, N. L., Chan, A. W. H., Feingold, G., Flagan, R. C., and Seinfeld, J. H.: Particulate
708 organic acids and overall water-soluble aerosol composition measurements from the 2006 Gulf of
709 Mexico Atmospheric Composition and Climate Study (GoMACCS), Journal of Geophysical
710 Research-Atmospheres, 112, 10.1029/2007jd008537, 2007b.
711 Sorooshian, A., Wang, Z., Coggon, M. M., Jonsson, H. H., and Ervens, B.: Observations of Sharp
712 Oxalate Reductions in Stratocumulus Clouds at Variable Altitudes: Organic Acid and Metal
713 Measurements During the 2011 E-PEACE Campaign, Environmental Science & Technology, 47,
714 7747-7756, 10.1021/es4012383, 2013.
715 Stone, E. A., Hedman, C. J., Zhou, J. B., Mieritz, M., and Schauer, J. J.: Insights into the nature of
716 secondary organic aerosol in Mexico City during the MILAGRO experiment 2006, Atmospheric
717 Environment, 44, 312-319, 10.1016/j.atmosenv.2009.10.036, 2010.
718 Sullivan, R. C., and Prather, K. A.: Investigations of the diurnal cycle and mixing state of oxalic acid in
719 individual particles in Asian aerosol outflow, Environmental Science & Technology, 41,
720 8062-8069, 10.1021/es071134g, 2007a.
721 Sullivan, R. C., and Prather, K. A.: Investigations of the diurnal cycle and mixing state of oxalic acid in
722 individual particles in Asian aerosol outflow, Environmental Science Technology, 41, 8062-8069,
723 2007b.
724 Surratt, J. D., Kroll, J. H., Kleindienst, T. E., Edney, E. O., Claeys, M., Sorooshian, A., Ng, N. L.,
725 Offenberg, J. H., Lewandowski, M., Jaoui, M., Flagan, R. C., and Seinfeld, J. H.: Evidence for
726 organosulfates in secondary organic aerosol, Environmental Science & Technology, 41, 517-527,
727 10.1021/Es062081q, 2007.
728 Surratt, J. D., Gomez-Gonzalez, Y., Chan, A. W. H., Vermeylen, R., Shahgholi, M., Kleindienst, T. E.,
729 Edney, E. O., Offenberg, J. H., Lewandowski, M., Jaoui, M., Maenhaut, W., Claeys, M., Flagan, R.
730 C., and Seinfeld, J. H.: Organosulfate formation in biogenic secondary organic aerosol, Journal of
731 Physical Chemistry A, 112, 8345-8378, Doi 10.1021/Jp802310p, 2008.
732 Tan, Y., Perri, M. J., Seitzinger, S. P., and Turpin, B. J.: Effects of Precursor Concentration and Acidic
733 Sulfate in Aqueous Glyoxal-OH Radical Oxidation and Implications for Secondary Organic
734 Aerosol, Environmental Science & Technology, 43, 8105-8112, 10.1021/Es901742f, 2009.
735 ten Brink, H., Otjes, R., Jongejan, P., and Slanina, S.: An instrument for semi-continuous monitoring of
736 the size-distribution of nitrate, ammonium, sulphate and chloride in aerosol, Atmospheric
737 Environment, 41, 2768-2779, 2007.

738 Tong, H. J., Arangio, A. M., Lakey, P. S. J., Berkemeier, T., Liu, F. B., Kampf, C. J., Brune, W. H.,
739 Poschl, U., and Shiraiwa, M.: Hydroxyl radicals from secondary organic aerosol decomposition in
740 water, Atmospheric Chemistry and Physics, 16, 1761-1771, 10.5194/acp-16-1761-2016, 2016.
741 van Pinxteren, D., Neususs, C., and Herrmann, H.: On the abundance and source contributions of
742 dicarboxylic acids in size-resolved aerosol particles at continental sites in central Europe,
743 Atmospheric Chemistry and Physics, 14, 3913-3928, 10.5194/acp-14-3913-2014, 2014.
744 Wang, G., Cheng, C., Meng, J., Huang, Y., Li, J., and Ren, Y.: Field observation on secondary organic
745 aerosols during Asian dust storm periods: Formation mechanism of oxalic acid and related
746 compounds on dust surface, Atmospheric Environment, 113, 169-176, 2015.
747 Wang, G., Zhang, R., Gomez, M. E., Yang, L., Levy Zamora, M., Hu, M., Lin, Y., Peng, J., Guo, S.,
748 Meng, J., Li, J., Cheng, C., Hu, T., Ren, Y., Wang, Y., Gao, J., Cao, J., An, Z., Zhou, W., Li, G.,
749 Wang, J., Tian, P., Marrero-Ortiz, W., Secrest, J., Du, Z., Zheng, J., Shang, D., Zeng, L., Shao, M.,
750 Wang, W., Huang, Y., Wang, Y., Zhu, Y., Li, Y., Hu, J., Pan, B., Cai, L., Cheng, Y., Ji, Y., Zhang, F.,
751 Rosenfeld, D., Liss, P. S., Duce, R. A., Kolb, C. E., and Molina, M. J.: Persistent sulfate formation
752 from London Fog to Chinese haze, Proceedings of the National Academy of Sciences, 113,
753 13630-13635, 10.1073/pnas.1616540113, 2016.
754 Wang, G. H., Kawamura, K., Cheng, C. L., Li, J. J., Cao, J. J., Zhang, R. J., Zhang, T., Liu, S. X., and
755 Zhao, Z. Z.: Molecular Distribution and Stable Carbon Isotopic Composition of Dicarboxylic
756 Acids, Ketocarboxylic Acids, and alpha-Dicarbonyls in Size-Resolved Atmospheric Particles
757 From Xi'an City, China, Environmental Science & Technology, 46, 4783-4791,
758 10.1021/es204322c, 2012.
759 Wang, J. Y., Wang, G. H., Gao, J., Wang, H., Ren, Y. Q., Li, J. J., Wu, C., Zhang, L., Wang, S. L., and
760 Chai, F. H.: Concentrations and stable carbon isotope compositions of oxalic acid and related SOA
761 in Beijing before, during and after the 2014 APEC, Atmospheric Chemistry and Physics 17,
762 981-992, 2017.
763 Weller, C., Tilgner, A., Brauer, P., and Herrmann, H.: Modeling the Impact of Iron-Carboxylate
764 Photochemistry on Radical Budget and Carboxylate Degradation in Cloud Droplets and Particles,
765 Environmental Science & Technology, 48, 5652-5659, 10.1021/es4056643, 2014.
766 Wonaschuetz, A., Sorooshian, A., Ervens, B., Chuang, P. Y., Feingold, G., Murphy, S. M., de Gouw, J.,
767 Warneke, C., and Jonsson, H. H.: Aerosol and gas re-distribution by shallow cumulus clouds: An
768 investigation using airborne measurements, Journal of Geophysical Research-Atmospheres, 117,
769 10.1029/2012jd018089, 2012.
770 Xue, J., Lau, A. K. H., and Yu, J. Z.: A study of acidity on PM2.5 in Hong Kong using online ionic
771 chemical composition measurements, Atmospheric Environment, 45, 7081-7088,
772 10.1016/j.atmosenv.2011.09.040, 2011.
773 Yang, F., Chen, H., Wang, X., Yang, X., Du, J., and Chen, J.: Single particle mass spectrometry of
774 oxalic acid in ambient aerosols in Shanghai: Mixing state and formation mechanism, Atmospheric
775 Environment, 43, 3876-3882, 2009.
776 Yao, X. H., Fang, M., and Chan, C. K.: Size distributions and formation of dicarboxylic acids in
777 atmospheric particles, Atmospheric Environment, 36, 2099-2107, 2002.
778 Yao, X. H., Lau, A. P. S., Fang, M., Chan, C. K., and Hu, M.: Size distributions and formation of ionic
779 species in atmospheric particulate pollutants in Beijing, China: 2 - dicarboxylic acids,
780 Atmospheric Environment, 37, 3001-3007, 10.1016/s1352-2310(03)00256-5, 2003.
781 Yu, J. Z., Huang, X. F., Xu, J. H., and Hu, M.: When aerosol sulfate goes up, so does oxalate:

Implication for the formation mechanisms of oxalate, Environmental Science & Technology, 39, 128-133, 10.1021/Es049559f, 2005.

Yu, L., Smith, J., Laskin, A., Anastasio, C., Laskin, J., and Zhang, Q.: Chemical characterization of SOA formed from aqueous-phase reactions of phenols with the triplet excited state of carbonyl and hydroxyl radical, Atmospheric Chemistry and Physics, 14, 13801-13816, 10.5194/acp-14-13801-2014, 2014.

Zauscher, M. D., Wang, Y., Moore, M. J. K., Gaston, C. J., and Prather, K. A.: Air Quality Impact and Physicochemical Aging of Biomass Burning Aerosols during the 2007 San Diego Wildfires, Environmental Science & Technology, 47, 7633-7643, 10.1021/es4004137, 2013.

Zhang, G., Bi, X., Li, L., Chan, L. Y., Li, M., Wang, X., Sheng, G., Fu, J., and Zhou, Z.: Mixing state of individual submicron carbon-containing particles during spring and fall seasons in urban Guangzhou, China: a case study, Atmospheric Chemistry and Physics, 13, 4723-4735, 2013.

Zhang, G., Bi, X., He, J., Chen, D., Chan, L. Y., Xie, G., Wang, X., Sheng, G., Fu, J., and Zhou, Z.: Variation of secondary coatings associated with elemental carbon by single particle analysis, Atmospheric Environment, 92, 162-170, 2014.

Zhang, R., Wang, G., Guo, S., Zamora, M. L., Ying, Q., Lin, Y., Wang, W., Hu, M., and Wang, Y.: Formation of urban fine particulate matter, Chem Rev, 115, 3803-3855, 2015.

Zhou, Y., Huang, X. H., Bian, Q., Griffith, S. M., Louie, P. K., and Yu, J. Z.: Sources and atmospheric processes impacting oxalate at a suburban coastal site in Hong Kong: Insights inferred from 1 year hourly measurements, Journal of Geophysical Research: Atmospheres, 120, 9772-9788, 2015.

Tables and Figures

Table list:

Table 1. Summary of major groups of oxalic acid-containing particles in summer and winter in PRD, China.

Table 2. The abundance of major particle types in total oxalic acid-containing particles during the episode in winter (2/8/2015).

Figure caption:

Figure 1. Temporal variations of total detected particles and oxalic acid containing particles during whole sampling periods in Heshan, China: (a) hourly variations of $PM_{2.5}$ mass concentration, total detected particle counts, oxalic acid containing particles, ratio of oxalic acid-containing/total particles and major types of oxalic acid containing particles; (b) variation patterns of relative abundance of major types of oxalic acid containing particles.

Figure 2. The averaged positive and negative ion mass spectra of oxalic acid containing particles is investigated in summer and winter: (a) summer positive, (b) summer negative, (c) winter positive, (d) winter negative. The color bars represent each peak area corresponding to specific fraction in individual particles.

Figure 3. (a) Mixing state of oxalic acid with sulfate, nitrate and ammonium in oxalic acid-containing particles; (b) Linear correlation between NH_4^+-containing oxalic acid particles and the total oxalic acid particles in summer; (c) Linear correlation between NH_4^+-containing oxalic acid particles and the total oxalic acid particles in winter. Abbreviations: C_2-NH_4^+ represents the NH_4^+-containing oxalic acid particles, and same expressions for C_2-SO_4^{2-} and C_2-NO_3^-.

Figure 4. Unscaled size-resolved number distributions of major types of oxalic acid particles in summer and winter.

Figure 5. Temporal variations of O_3 concentrations, oxalic acid particles, malonic acid particles and heavy metal type of oxalic acid particles during the entire sampling period in Heshan, China.

Figure 6. The averaged digitized positive and negative ion mass spectra of heavy metal type of oxalic acid-containing particles in summer.

Figure 7. The diurnal variations of O_3 concentration, oxalic acid particles, HM group particles and in-situ pH (pH_{is}) from July 28 to August 1 in 2014.

Figure 8. The diurnal variations of peak area of iron (m/z=56) and oxalic acid (m/z=-89) in the HM type oxalic acid particles from July 28 to August 1, 2014.

Figure 9. The temporal variations of peak area of nitrate, sulfate and oxalic acid, and the relative acidity ratio (R_{ra}) in carbonaceous type oxalic acid particles in winter.

Figure 10. The comprehensive study of oxalic acid particles increase on Feb 8, 2015: (a) The digitized positive and negative ion mass spectrum of oxalic acid particles during the episode; (b) Linear regression between total oxalic acid particles and organosulfate-containing oxalic acid particles (m/z -155).

Table 1. Summary of major groups of oxalic acid-containing particles in summer and winter in PRD, China.

	Summer(7/18-8/1, 2014)		Winter(1/27-2/8, 2015)	
Particle type	Count	Percentage, %	Count	Percentage, %
EC	1473	11.2	3161	15.4
ECOC	41	0.3	2233	10.9
OC	473	3.6	1922	9.4
BB	1702	13.0	4953	24.2
HM	4104	31.3	3124	15.2
Sec	2511	19.2	2192	10.7
NaK	303	2.3	17	0.1
Dust	1139	8.7	1888	9.2

Abbreviations of major particle types: elemental carbon (EC), elemental and organic carbon (ECOC), organic carbon (OC), biomass burning (BB), heavy metal (HM), secondary (Sec), sodium and potassium (NaK) and dust (Dust).

Table 2. The abundance of major particle types in total oxalic acid-containing particles during the episode in winter (2/8/2015).

	EC	ECOC	OC	BB	Sec	HM	Dust	other
Count	1250	604	326	1320	856	377	814	132
Percentage, %	22.0	10.6	5.7	23.2	15.1	6.6	14.3	2.3

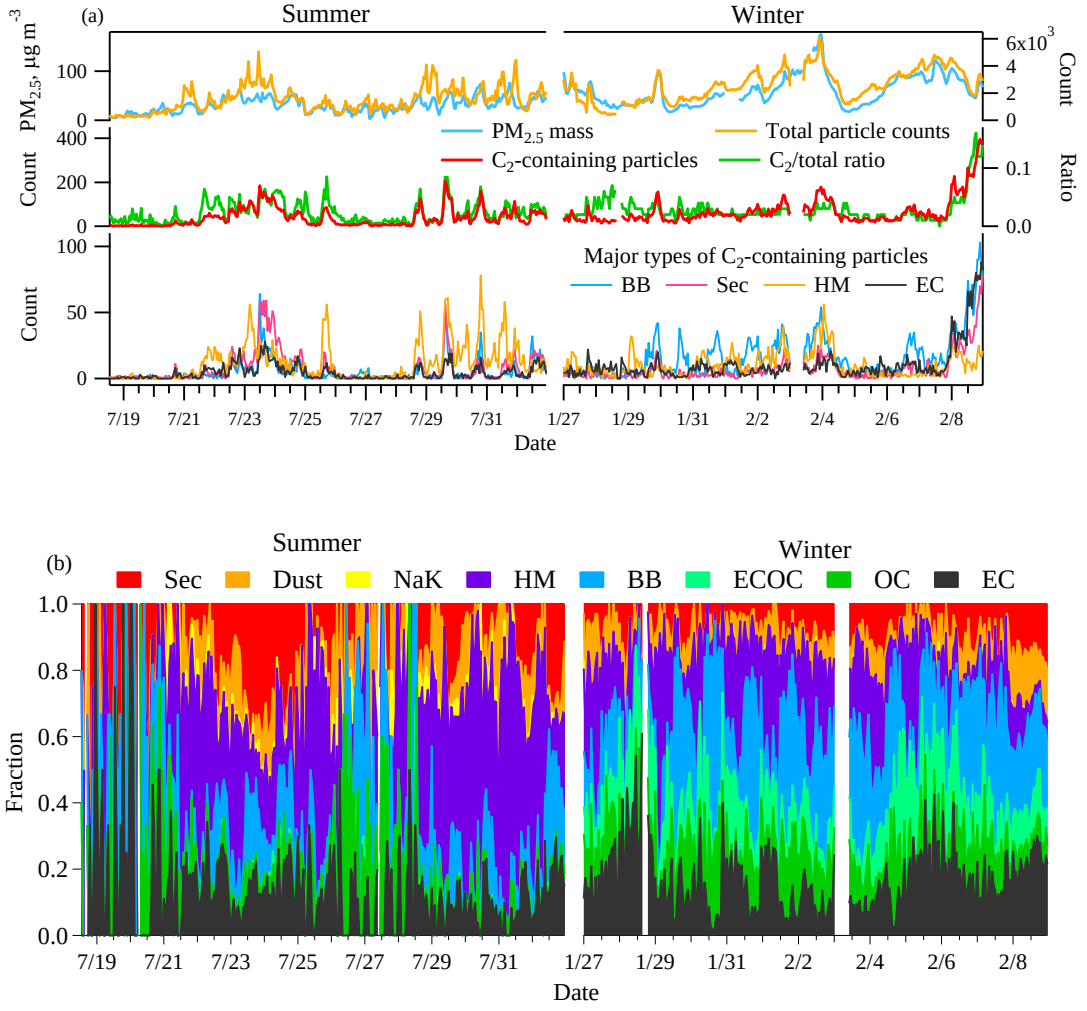

Figure 1. Temporal variations of total detected particles and oxalic acid containing particles during whole sampling periods in Heshan, China: (a) hourly variations of $PM_{2.5}$ mass concentration, total detected particle counts, oxalic acid containing particles, ratio of oxalic acid-containing/total particles and major types of oxalic acid containing particles; (b) variation patterns of relative abundance of major types of oxalic acid containing particles. Abbreviations of major particle types: elemental carbon (EC), organic carbon (OC), elemental and organic carbon (ECOC), biomass burning (BB), heavy metal (HM), secondary (Sec), sodium and potassium (NaK) and dust.

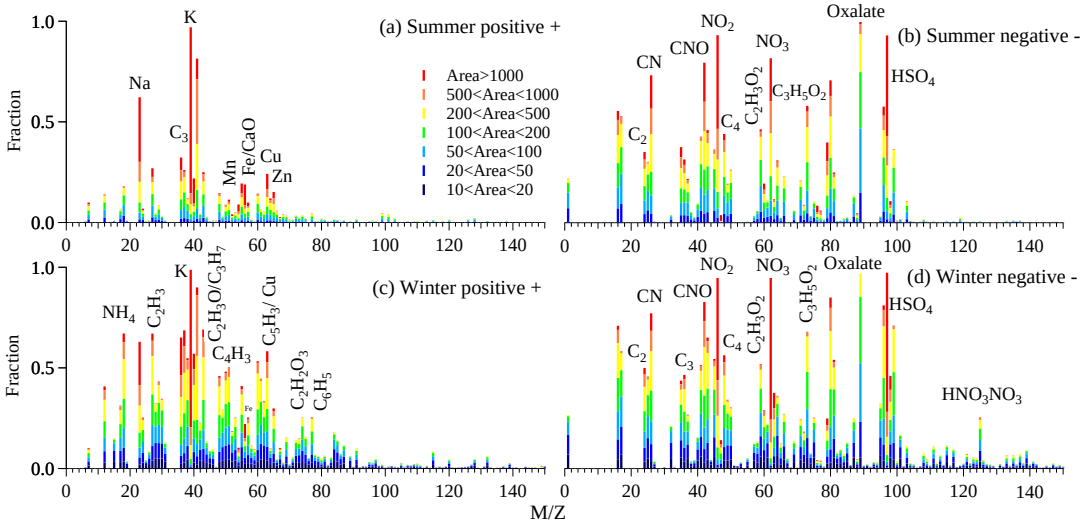

Figure 2. The averaged positive and negative ion mass spectra of oxalic acid containing particles is investigated in summer and winter: (a) summer positive, (b) summer negative, (c) winter positive, (d) winter negative. The color bars represent each peak area corresponding to specific fraction in individual particles.

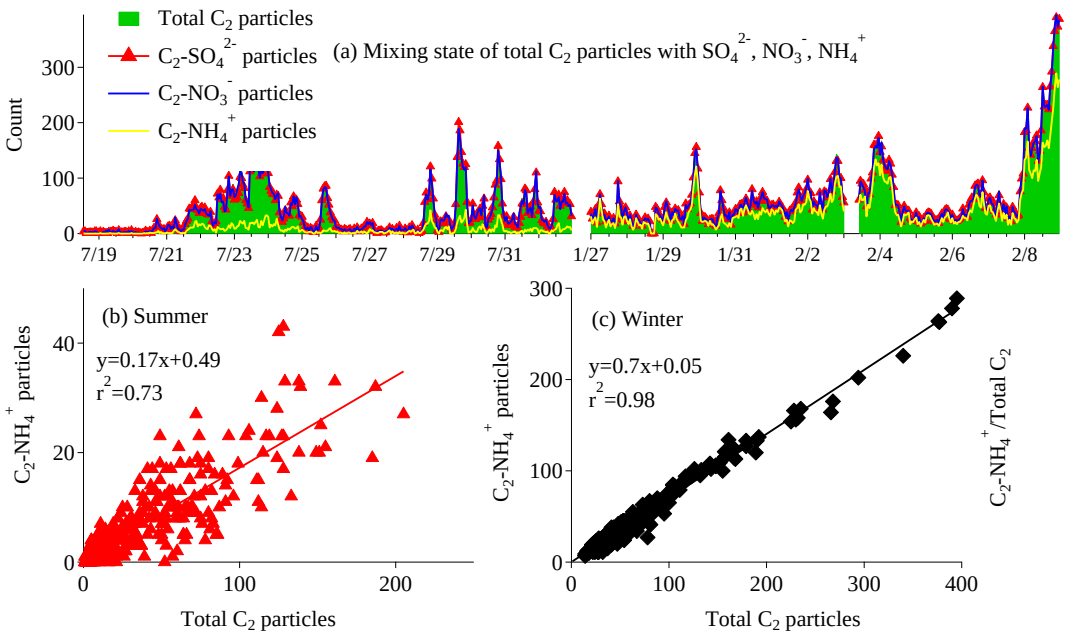

Figure 3. (a) Mixing state of oxalic acid with sulfate, nitrate and ammonium in oxalic acid-containing particles; (b) Linear correlation between NH_4^+-containing oxalic acid particles and the total oxalic acid particles in summer; (c) Linear correlation between NH_4^+-containing oxalic acid particles and the total oxalic acid particles in winter. Abbreviations: C_2-NH_4^+ represents the NH_4^+-containing oxalic acid particles, and same expressions for C_2-SO_4^{2-} and C_2-NO_3^-.

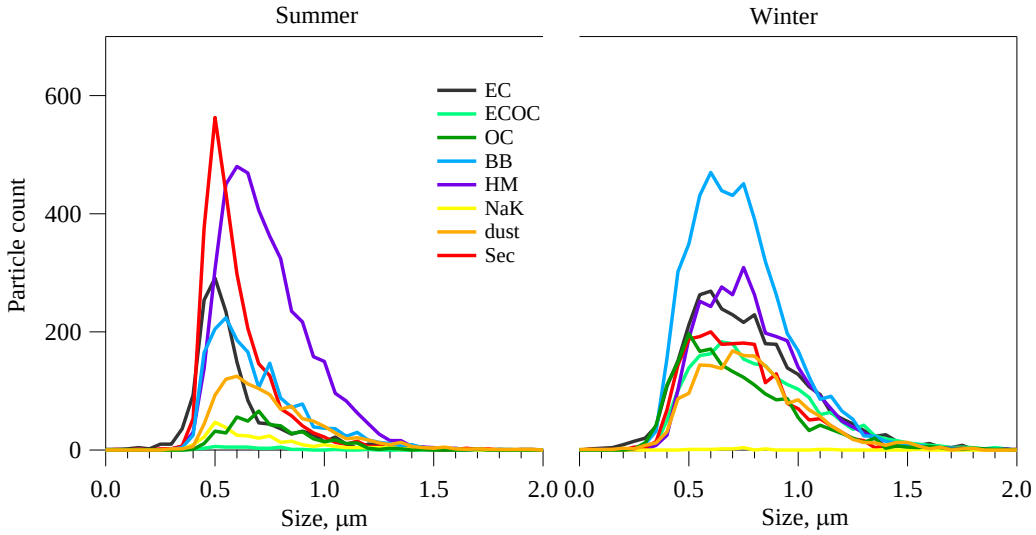

Figure 4. Unscaled size-resolved number distributions of major types of oxalic acid particles in summer and winter. Abbreviations of major particle types: elemental carbon (EC), organic carbon (OC), elemental and organic carbon (ECOC), biomass burning (BB), heavy metal (HM), secondary (Sec), sodium and potassium (NaK) and dust.

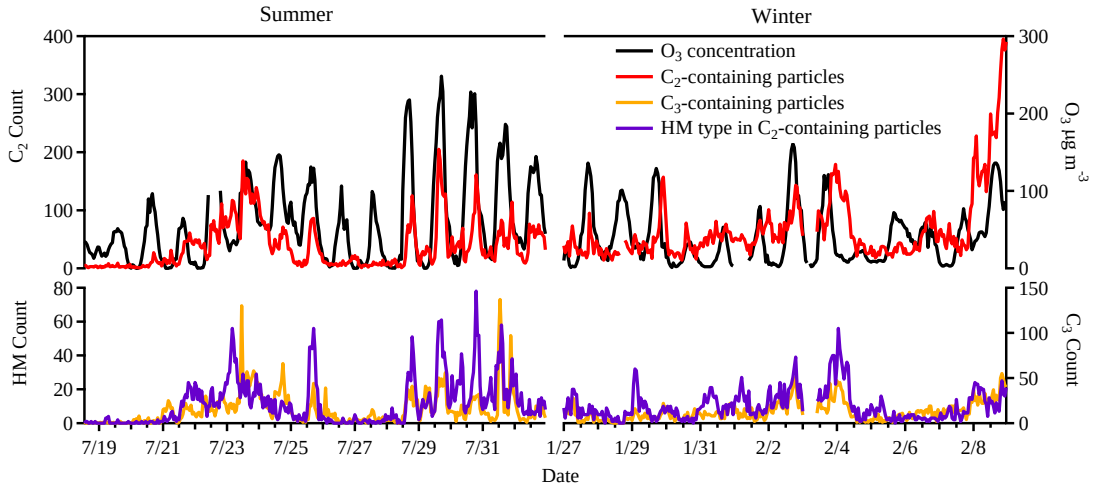

Figure 5. Temporal variations of O_3 concentrations, oxalic acid particles, malonic acid particles and heavy metal type of oxalic acid particles during the entire sampling period in Heshan, China.

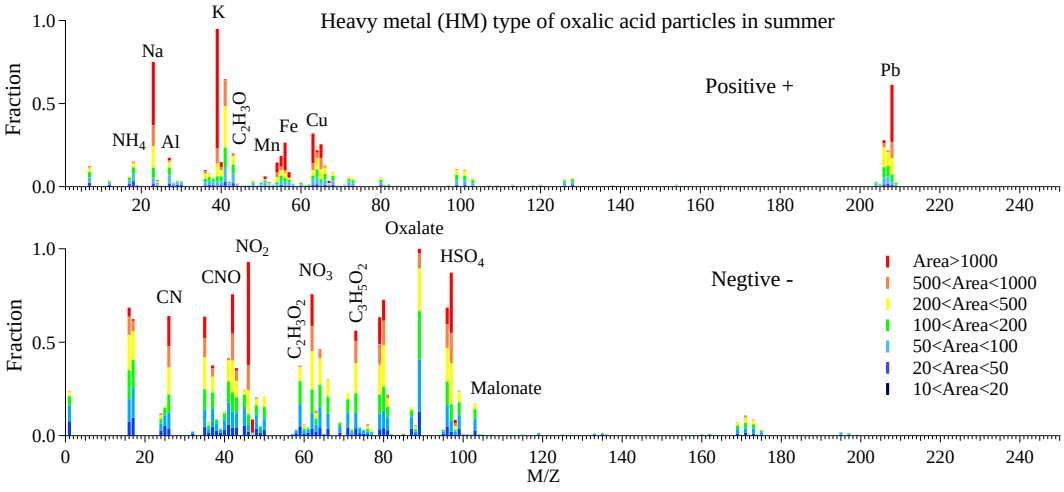

Figure 6. The averaged digitized positive and negative ion mass spectra of heavy metal type of oxalic acid-containing particles in summer.

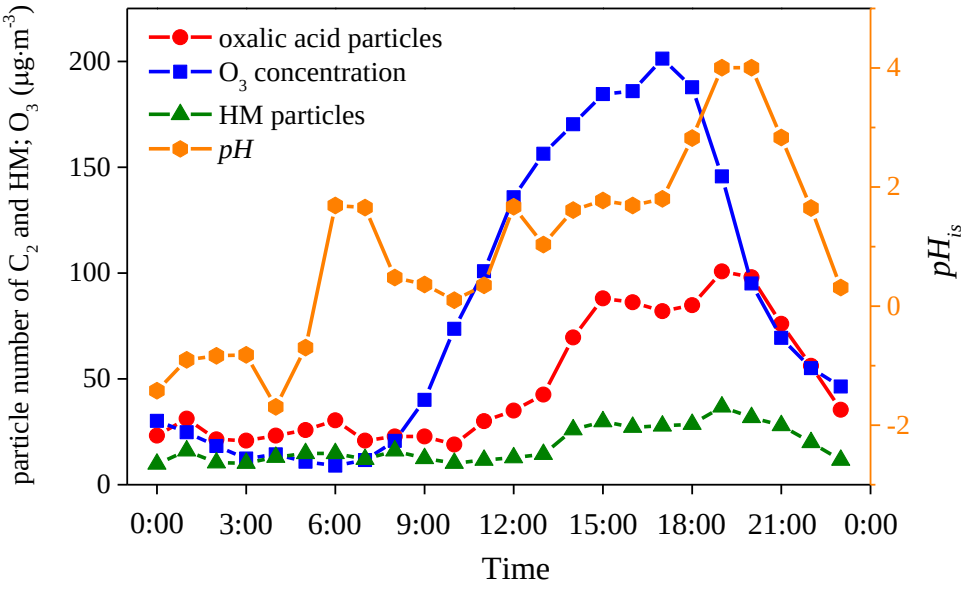

Figure 7. The diurnal variations of O_3 concentration, oxalic acid particles, HM group particles and in-situ pH (pH_{is}) from July 28 to August 1 in 2014.

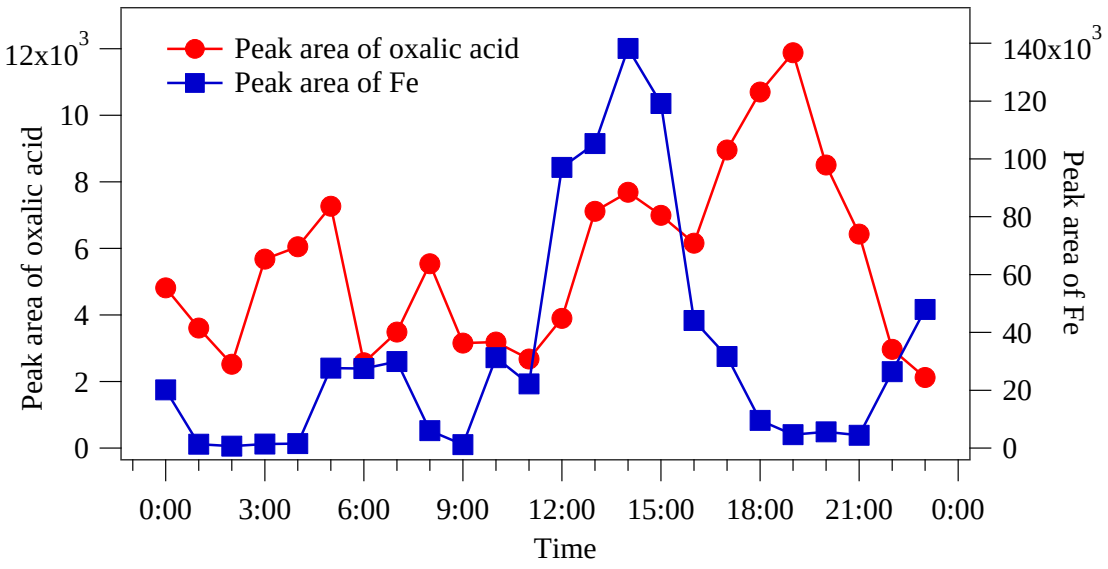

Figure 8. The diurnal variations of peak area of iron (m/z=56) and oxalic acid (m/z=-89) in the HM type oxalic acid particles from July 28 to August 1, 2014.

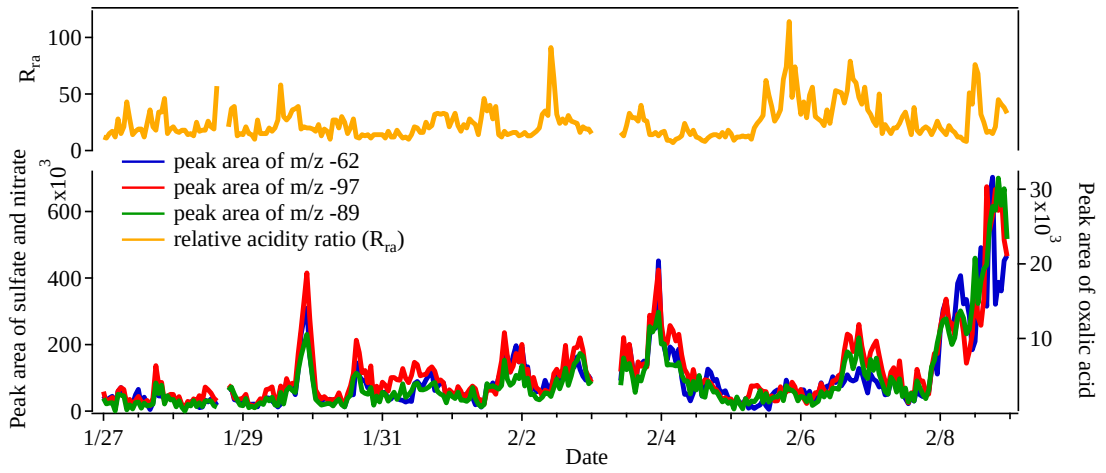

Figure 9. The temporal variations of peak area of nitrate, sulfate and oxalic acid, and the relative acidity ratio (R_{ra}) in carbonaceous type oxalic acid particles in winter.

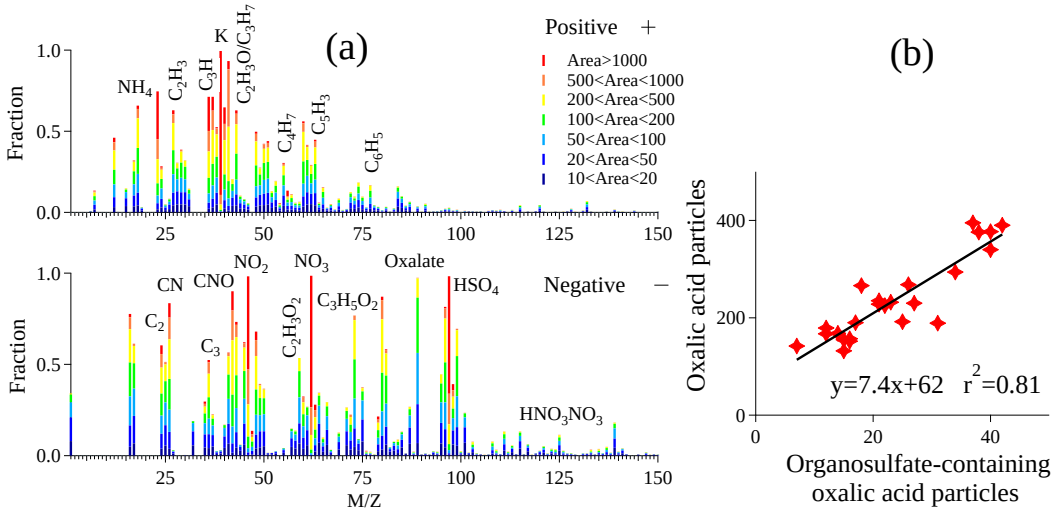

Figure 10. The comprehensive study of oxalic acid particles increase on Feb 8, 2015: (a) The digitized positive and negative ion mass spectrum of oxalic acid particles during the episode; (b) Linear regression between total oxalic acid particles and organosulfate-containing oxalic acid particles (m/z -155).